University of Pittsburgh

ORTHOPAEDIC ROBOTICS LABORATORY

2015 summer undergraduate abstract booklet

PITT | SWANSON ENGINEERING
BIOENGINEERING

ORL
Orthopaedic Robotics Laboratory

DEPARTMENT OF ORTHOPAEDIC SURGERY
UNIVERSITY OF PITTSBURGH

FOREWARD

The Orthopaedic Robotics Laboratory is a collaborative effort between the Department of Bioengineering and Department of Orthopaedic Surgery. The mission of the ORL is the prevention of degenerative joint diseases by improving diagnostic, repair, and rehabilitation procedures for musculoskeletal injuries using state-of-the-art robotic technology. The ORL would like to commend the work of the undergraduate students during the summer of 2015. Students made significant impacts in the study of ankle, knee, wrist, and shoulder degenerative diseases. The work of our students, with the help of our mentors, contributes greatly to the world of Orthopaedic Research and to all patients who benefit.

Our team

Laura Bechard
Class of 2016
Bioengineering
University of
Pittsburgh

Chris Como
Class of 2017
Bioengineering
University of
Michigan

Trenton Gilstrap
Class of 2016
Bioengineering
University of
Pittsburgh

Samik Patel
Class of 2018
Bioengineering
University of
Pittsburgh

Audra Sawyer
Class of 2015
Bioengineering
University of
Virginia

Stephanie Sexton
Class of 2016
Bioengineering
University of
Pittsburgh

Joe Takahashi
Class of 2016
Bioengineering
University of
Pittsburgh

Table of contents

Design of Customized Lower Leg Specimen Fixtures for 6 DOF Robotic Testing System

Bechard, LE[1]; Bell, KM[1]; Hogan, MV[2,1]; Debski, RE[1,2]

1. Department of Bioengineering, University of Pittsburgh, Pittsburgh, PA
2. Department of Orthopaedic Surgery, University of Pittsburgh, Pittsburgh, PA

Introduction: High ankle sprains, or ankle syndesmosis injuries, account for 10% of all ankle sprains [1]. The most common mechanisms of injury are external rotation and hyper-dorsiflexion of the ankle joint. The ankle syndesmosis restrains tibiofibular motion, which is vital to ankle stability [2]. Previous studies of ankle syndesmosis injuries have relied on static trials and manually applied loads. Additionally, previous studies have utilized sectioned lower leg specimens, which disrupt the proximal syndesmosis.

The MJT Model FRS2010 robotic testing system is capable of dynamic manipulation repeatable to 0.001 mm. The robotic testing system is currently used to study biomechanics of the knee, shoulder, and spine. However, the current system is incapable of rigidly fastening a full lower leg specimen for testing. The objective of this project was to design and test the rigidity of a customized clamping system for fastening a full lower leg specimen to the robotic testing system.

Design Criteria: In addition to accommodating a full lower leg specimen, the customized lower leg specimen fixtures must not disrupt the syndesmosis or inhibit fibular motion. Within the size constraints of the robotic testing system, the clamps must be adjustable to specimen height without preventing motion of the robotic testing system. The customized lower leg fixtures must rigidly fasten both the tibia and the calcaneus. Expected tibiofibular motion is approximately 0.43 – 4.28 mm with inhibited fibular motion [1]. Therefore, in order to qualify the fixture as rigid, movement of the specimen and fixture must be less than 0.5 mm during testing. Additionally, the fixture must also prevent bending of the tibia. Movement of the medial malleolus with respect to the tibia mid-shaft must be less than 0.5 mm during testing.

Final Design: The final clamp design consists of both mass-produced and custom designed materials. The lower leg specimen is fastened to the robotic testing system with the proximal tibia inferior to the distal tibia. The proximal tibia is fastened with two screws to a custom designed plate (Figure 1D) which is fastened directly to the base of the robotic testing system.

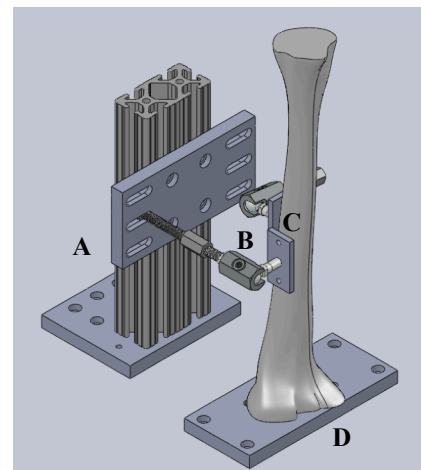**Figure 1**: Final customized fixture design to fasten full lower leg specimen to robotic testing system. A) 8020 T-slotted aluminum construct. B) Lockable ball joint. C) Small tibia plate. D) Proximal tibia plate.

Two small custom designed plates (Figure 1C) are fastened to the tibia approximately mid-shaft using bone screws. The plates minimize the amount of soft tissue dissection and increase

stability of the bone-plate joint. The two plates are attached to lockable ball joints (Figure 1B) to allow multiple fastening options. The lockable ball joint is fastened to a vertical construct which consists of custom base, 8020 T-slotted aluminum, and custom adapter plate (Figure 1A).

The ankle joint is manipulated through the calcaneus. Screws are inserted in the calcaneus through the talus. Approximately 4 cm of the head of the screw is left exposed. The entire screw-calcaneus complex is potted in bondo putty (3M, Saint Paul, MN). The cylindrical form is fastened the robotic testing system using an existing clamp originally designed for knee joint testing (Figure 2).
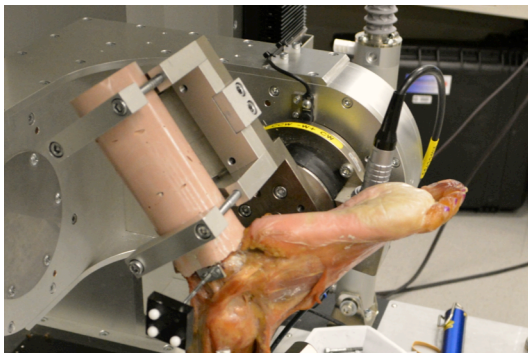

Figure 2: Existing clamp used to fasten potted

Rigidity Analysis: One fresh frozen lower leg (shank and foot) cadaveric specimen was fastened to the MJT FRS 2010 robotic testing system (Technology Services Ltd., Chino, Japan) using the fabricated fixtures. At neutral position, a mechanical digitizer (Faro Arm, Lake Mary, FL) was used to collect location of anatomical and clamp landmarks: calcaneus clamp bolt, calcaneus anatomical bolt, tibia clamp bolt, medial malleolus, and tibia mid-shaft bolt. The mechanical digitizer is accurate to 0.05 mm. Location of the landmarks was recollected at various loading conditions representing normal ankle motion and injury states: 10 Nm external rotation at 0° flexion, 10 Nm at 10° dorsiflexion, 10 Nm external rotation at 30° plantarflexion, and 10 Nm dorsiflexion. In order to quantify rigidity, the three-dimensional distance between calcaneal landmarks and between tibial landmarks is calculated. MATLAB (MathWorks, Natick, MA) was used to determine distance between the calcaneus clamp bolt and calcaneus anatomical bolt, the tibia clamp to the medial malleolus, the tibia clamp and the tibia mid-shaft bolt, and the medial malleolus and the tibia mid-shaft bolt.

The change in distance between clamp and specimen landmarks ranged from 0.00-0.46 mm. The average change in distance was 0.29 mm. The change in distance between the medial malleolus and the tibia mid-shaft ranged from 0.03-0.26 mm. The average change was 0.12 mm. Results are summarized in Table 1.

Conclusion: The change in distance between clamp and specimen landmarks met the design criteria by remaining under 0.5 mm for all loading conditions. The fixture also prevented bending of the tibia in all trials. Therefore, the

Table 1: Change in three-dimensional distance between digitized landmarks

Flexion	External Rotation (Nm)	Calcaneus clamp - specimen (mm)	Tibia clamp – medial malleolus (mm)	Tibia clamp – tibia mid-shaft (mm)	Medial malleolus – tibia mid-shaft (mm)
0°	10	0.38	0.00	0.13	0.03
10°	10	0.30	0.02	0.12	0.04
-30°	10	0.46	0.16	0.18	0.15
10 Nm	0	0.24	0.24	0.10	0.26

clamp can be considered a rigid fixture for full lower leg specimens. The study is limited by the limited volume the mechanical digitizer is able to digitize. Due to the size of the specimen, it was impossible to digitize a landmark on the proximal tibia. A proximal tibia landmark would have been beneficial in further validating the use of the fixture to prevent tibia bending.

Significance: The design of a full lower leg specimen fixture enables utilization of the MJT Model FRS2010 robotic testing in ankle syndesmosis studies. In conjunction with a motion tracking system, tibiofibular motion in intact and injured states can be compared. Further, different types of syndesmosis surgical fixation methods can be investigated in vitro. The study can help improve rehabilitation and patient outcomes after ankle syndesmosis surgeries.

References: [1] Markolf, et al. FAI. 2012. [2] Van Heest, et al. JBJS. 2014.

Restoration of Shoulder and Knee Testing Apparatus

Como, CJ.; Gilstrap, TA.; Debski, RE.

Orthopaedic Robotics Laboratory, Departments of Orthopaedic Surgery and Bioengineering, University of Pittsburgh, Pittsburgh, PA

Introduction: The Shoulder Testing Apparatus Revision IV (STAR-IV) was designed in 2005 to improve on a previous dynamic shoulder testing apparatus [1]. Originally built to simulate joint kinematics of the shoulder joint, the STAR-IV now has the ability to test the kinematics of the knee joint. STAR-IV analyzes forces and kinematics involved in shoulder and knee motion to improve rehab protocols and evaluate surgical procedures. STAR-IV utilizes six actuators to create dynamic motion at the glenohumeral or patellofemoral joint. Cables attached to muscle tendons in the shoulder or knee are controlled by the actuators to create motion at the joint. However, about three years ago the STAR-IV computer stopped functioning and resulted in no control of the actuators. In addition, some of the control hardware and software were outdated and there was broken equipment that needed fixed. This project planned to reestablish control of the actuators with newly installed hardware and develop a user-friendly interface in LabVIEW™.

In order to accomplish this goal, there was a series of steps that needed to be taken:

1. Install new hardware / software
2. Update wiring of hardware enclosure
3. Regain motion control of actuators through ACR-View
4. Control actuators in LabVIEW™
5. Create user interface in LabVIEW™

Upgraded Hardware and Setup: In order to gain control of the actuators once again, the system required hardware modifications. First, a PCI-6071E DAQ card, wired to an ATI-660-60 load cell on the shoulder mount, was directly installed into the computer. Then, a new Parker ACR 9630 motion controller was mounted directly in the hardware enclosure to replace the old breakout box. The motion controller was wired via 26-pin cable to six Aries servo drives.

Next, new Parker PIO modules were installed for the inputs and outputs of the system. These modules connect to the motion controller via CANopen connection. The analog inputs from the six MLP-300-CO load cells (one on each actuator) were then wired through six signal conditioners into the analog input PIO module. A 25-pin module was added to the hardware for the limit switches of the system. Finally, new load cell cables and a new limit switch were installed to replace previously broken equipment. **Figure 1** shows the updated hardware enclosure.

Development of a User-Friendly Interface in LabVIEW™: The ACR 9630 motion controller comes with a software program called ACR-View. ACR-View allows for user input and provides live feedback, such as load cell data. This software also allows the user to create programs and load them onto the motion controller. This feature will be utilized in the coding of LabVIEW™ for the user interface. Each component (load cell data, actuator movement, actuator current position, etc.) has an associated parameter in ACR-View. Incorporating these parameters into LabVIEW™ allows for monitoring and controlling the entire STAR-IV system. The six parameters shown in **Figure 2** obtain the current position of each actuator from ACR-View and allow the user to view the position in LabVIEW™. Using this parameter method for most aspects of the coding, a user-friendly interface was developed to obtain complete control of the actuators. With buttons directly available on the user interface, there is no setup required in ACR-View prior to testing. Live feedback, such as the current load on each actuator (axis), the current position of each axis, and the current velocity of each axis are also visible to the user. Status LEDs are also included, allowing for simple error handling and axis status feedback. In addition, the user has

control over any combination of axes with displacement or force control. For displacement control, the user simply enters a position for each axis they wish to move and click the move button. For force control, force feedback loops for each axis were created and loaded onto the motion controller in ACR-View. As far as testing goes, the user again picks the axis or axes under force control, defines the force set point, and starts force control once the load cells have been zeroed. **Figure 3** shows the user-friendly interface that was developed in LabVIEW™.

Calibration of STAR-IV System: To calibrate the system, the displacement transducers and load cells must be scaled correctly. The displacement transducers have a set 5.1 millimeters per revolution for the scale, so this was set in LabVIEW™. To scale the load cells, however, multiple steps are required. In the hardware enclosure, each signal conditioner has balance and gain offset knobs that must be set so that each load cell reads very close to zero with no load applied. Once these are set for all six signal conditioners, a scale must be found for the load cells in order for the load to be viewed in Newtons, rather than volts. To find this scale factor a spring scale was used. Weights were hung from the spring scale for validation. Then, the actuators were attached to the spring scales and moved to reach loads in increments of two pounds, all the way up to forty pounds. The voltage was recorded at each increment. The voltage vs. pounds data was plotted and a linear fit was used to find the slope. Once this volt per pound scale was obtained, it simply needed to be converted to volts per Newton. This value turned out to be 0.0126343 V/N and was set in the LabVIEW™ code.

Testing and Validation: After scales were obtained and programed in LabVIEW™ for the displacement transducers and load cells, validation data was obtained to assess the accuracy of the system. To test the displacement accuracy, a digital caliper was used to measure user-set distances for each actuator. It is important to note that the measurement with the caliper was taken without knowledge of the specified target distance of the actuator. Each actuator was +/- 0.1 millimeters of the target

displacement. The load cell scale was validated using spring scale readings and comparing each reading to the actual force in LabVIEW™. Again, the spring scale reading was taken blindly to the applied force. Since the spring scales used had human error in the reading and the load cells are capable of forces up to 300 pounds, the error of the load cells is higher than the error of the displacement transducers. However, even with more sources of error, the load cells were +/- 4 Newtons of the target load.

References: [1] Debski RE et al. *A New Dynamic Testing Apparatus To Study Glenohumeral Joint Motion* J. Biomechanics 1995; 28(7); 869-874
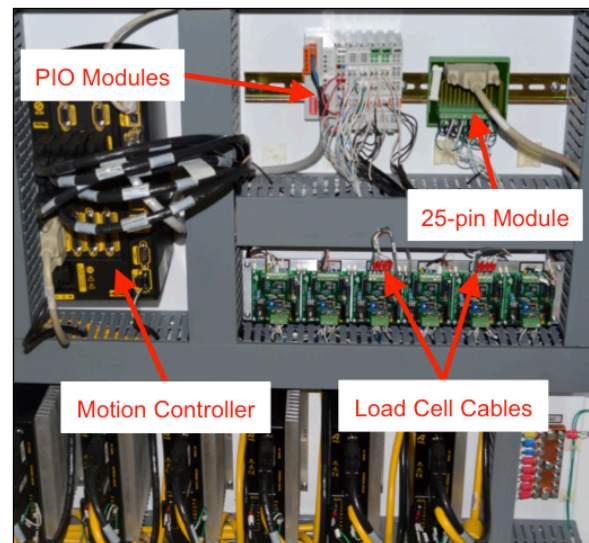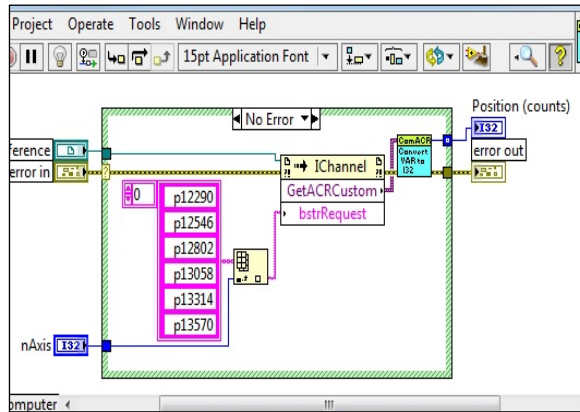

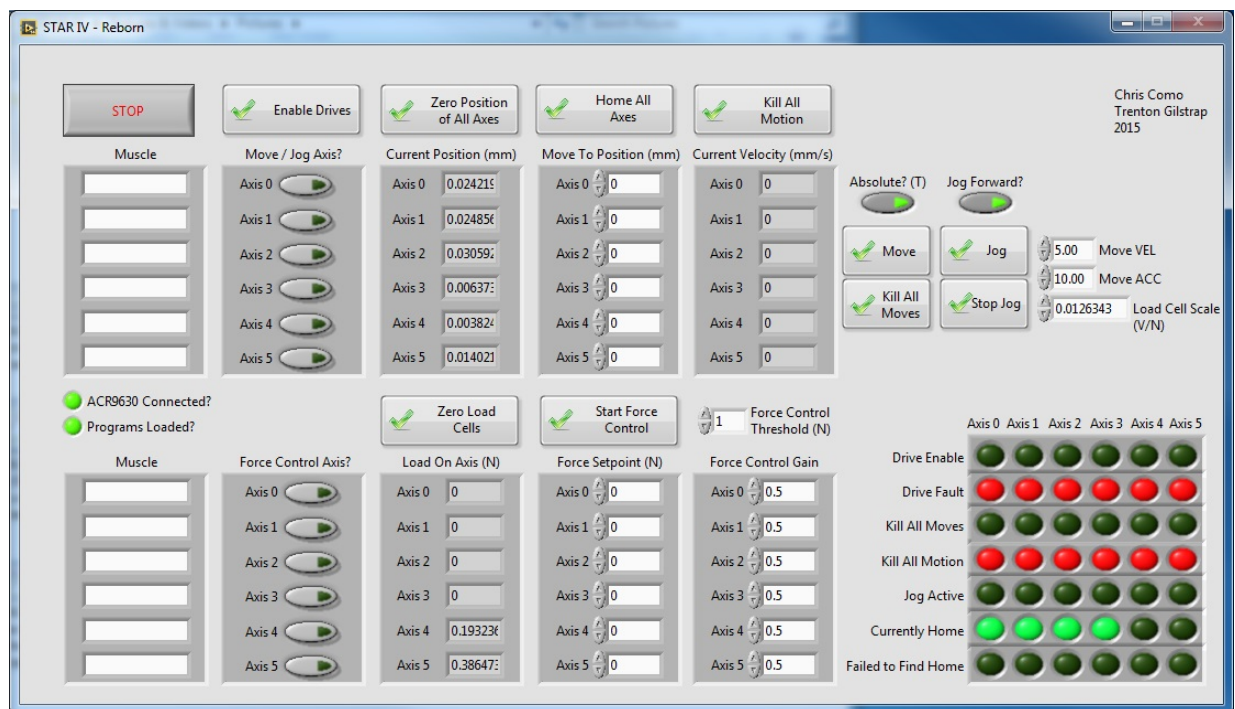**Figure 1: Hardware Enclosure Wiring**

Figure 2: LabVIEW™ Parameter Code

Figure 3: Developed User Interface in LabVIEW™

Analyzing Compression Forces of Internal Fixation Methods for Transvers Proximal Third Scaphoid Fractures

Samik D. Patel[1], Nate Tiedeken[2], Lars M. Qvick[2], Richard E. Debski[1], John Fowler[2]

[1]Department of Bioengineering, University of Pittsburgh, Pittsburgh, PA, United States.
[2]Department of Orthopaedic Surgery, University of Pittsburgh, Pittsburgh, PA, United States.

Introduction: Internal fixation used as treatment for scaphoid fractures has increased with advances in surgical techniques [1]. Proximal pole scaphoid fractures present a clinical challenge due to their lower success rate when cast immobilization and internal fixation are utilized [2]. Internal fixation with headless compression screws (HCS) provides a compressive force at the fracture site utilized to promote healing. Differences in geometrical design between HCS lead to differences in compression that vary based on the location of the fracture. As a result, the objective of this study is to analyze compression forces based on the screw type utilized for fixation and the location of the simulated transverse fracture.

Methods: Eighty-eight (n=4 for each of the 11 simulated fracture locations and for each of 2 screws) polyurethane foam blocks (Sawbone, Vashon Island, WA, USA) of 15 pounds per cubic foot density were cut to 28mm x 10mm x 10mm to represent a scaphoid. A fracture was simulated with a horizontal/transverse cut along the 28mm length of the block. The location of the horizontal cut varied from 2mm from the top edge of the block through 22mm, incrementing by 2mm for each possible fracture site. A HCS was inserted in the center of the scaphoid so that compression would occur at the simulated fracture site. The fully threaded 24mm Acutrak Standard HCS (Acumed, Hillsboro, OR, USA) and double threaded 24mm Fixos HCS (Stryker, Kalamazoo, MI, USA) were inserted according to manufacturer's protocol by a fellowship trained hand surgeon.

The amount of compression occurring at the fracture site was measured with sensors placed in between rubber and stainless steel (Figure 1). The FlexiForce Force Sensors
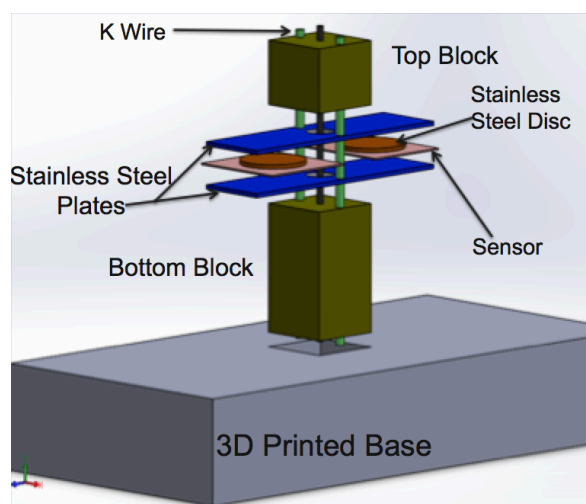

Figure 1: Experimental setup where the sizes of the top block and bottom block were varied to simulate different transverse fracture locations

(Tekscan Inc, Boston, MA, USA) measured the force that was applied over the pressure sensitive inking located within a silver sensing area. Stainless steel plates provided rigid support to the system, and the stainless steel discs allowed for force to be transferred directly over the sensing area of the sensors. The rubber provided the necessary deformation required for accuracy from the FlexiForce sensors. The sensors, rubber, and metal resulted in a simulated fracture thickness of 2.54mm. In addition, two K-wires were placed around the center of the screw to prevent rotation of the system when the screw was inserted over the central guide wire.

The HCS was inserted into the foam block until the screw head was flush with the foam block. Once the screw was inserted, ELF Software (Tekscan Inc, Boston, MA, USA) was utilized to record the force measured in the sensors. A paired t-test and two-way analysis of variance (ANOVA) were performed

to assess differences between the fixation methods at each of the simulated fracture locations. Significance was set at $p < 0.05$.

Results There was a significant effect of fracture location on compression ($p<.0001$), with a maximum difference in compression occurring between the fixated fracture located 22mm from the top edge of the top block generating 11.41% of the compression generated by a fixated fracture located 6mm from the top edge of the top block. There was also a significant difference in the compression generated between the Stryker and Acutrak screws at certain fracture locations. For a fracture located 2mm from the top edge of the top block, the Stryker screw generated significantly more compression ($p<.0001$) than the Acutrak screw with nearly ~3.63 times more compression (Table 1). The Acutrak screw generated significantly greater compression than Stryker screw with a 12mm top block fixation ($p<.0001$) and a 18mm top block fixation ($p<.001$).

Top Block Length (mm)	Acutrak	Stryker
	Average Compression (N)	Average Compression (N)
2*	6.3 ± 1.16	22.9 ± 3.33
4	29.1 ± 1.96	33.2 ± 3.70
6	42.9 ± 2.37	44.8 ± 3.08
8	40.3 ± 3.78	40.7 ± 1.19
10	44.4 ± 3.14	37.2 ± 2.82
12*	37.4 ± 2.24	23.7 ± 2.27
14	36.1 ± 2.71	33.3 ± 3.11
16	32.2 ± 5.13	27.2 ± 8.28
18*	15.6 ± 2.17	6.8 ± 2.23
20	8.7 ± 0.54	6.5 ± 5.12
22	6.1 ± 1.12	3.9 ± 0.86

Table 1: Displays average compression generated at each simulated fracture location (mean ± SD; *$p<.001$)

Discussion: This study examined the effects of screw type and transverse fracture location on compression force generated at the fracture site. The results of this study show that there is a difference in compression force generated based on the location of the fracture. Our data does not support previous literature on the distribution of compression force based on the fracture location for the Acutrak 2 HCS [3]. From our data, the Acutrak 2 generates greater compression force for the 6mm through 10mm top block lengths as opposed to the previously found bell curve distribution. In addition, our data has shown significant differences between the Acutrak HCS and the Stryker Fixos HCS at certain locations. The Stryker generated significantly greater compression at the 2mm top block length, which simulated a proximal pole fracture surgically repaired through the dorsal approach. The Acutrak screw generated significantly greater compression for certain fractures that could be repaired through the volar surgical technique located at the waist of the scaphoid. Our data supports previous literature showing the difference in compression between the Stryker HCS and Acutrak HCS for fractures that occur exactly at the waist (12mm top block length) [4].

Significance: The results of this study will provide surgeons with useful information that will help them in determining the optimal fixation technique for a scaphoid fracture based on the location of the fracture through either the volar or dorsal approach. The Stryker screw generates greater compression for fractures located at the proximal pole of the scaphoid, while the Acutrak screw generates greater compression for fractures located at the scaphoid waist.

References:
[1] Rhemrev S, Ootes D, Beeres F, Meylaerts S, Schipper I, "Current methods of diagnosis and treatment of scaphoid fractures" *International Journal of Emergency Medicine,* 2011 [2] Trumble M, Vo D, "Proximal Pole Scaphoid Fractures and Nonunion" *J of the American Society for Surgery of the Hand,* 2001, 155-171 [3] Sugathan H, Kilpatrick M, Joyce T, Harrison J, "A biomechanical study on variation of compressive force along the Acutrak 2 screw" *Injury Int. J. Care Injured,* 2012, 205-208 [4] Assari S, Darvish K, Ilyas A, "Biomechanical analysis of second-generation headless compression screws" *Injury, Int J. Care Injured*, 2012, 1159-1165

Learning the Standardized Pivot Shift Test by Use of Passive Education Tools

Jason P. Zlotnicki[1], Amir Ata Rahnemai-Azar[1], Audra M. Sawyer[1], Freddie H. Fu[1], Richard E. Debski[1], Volker Musahl[1]

[1]Orthopaedic Robotics Laboratory, Departments of Orthopaedic Surgery and Bioengineering, University of Pittsburgh, Pittsburgh, PA, United States

INTRODUCTION: The pivot shift test is the most specific diagnostic clinical test for anterior cruciate ligament (ACL) injury and relates to patient satisfaction and stability outcomes [1]. A 2D simple image analysis method has been implemented on a tablet computer to quantify the translation of the lateral knee compartment during the pivot shift test, with the goal of establishing a reproducible, quantitative measurement system allowing for an objective evaluation of test results [2]. However, this objective quantification is dependent upon standardization of the clinical pivot shift test required to generate the translation of the lateral knee compartment. Therefore, the objective of this study was to determine the ability of subjects of different skill levels to learn and perform ten standardized pivot shift tests [3, 4], compared to an experienced orthopaedic surgeon (gold standard). It was hypothesized that subjects would produce kinematics similar to the gold standard. Furthermore, after watching an instructional video, trials 6-10 would differ less from the gold standard compared to trials 1-5 of the standardized pivot shift test.

METHODS: Institutional review board approval was obtained for the use of human participants, with informed consent of each participant obtained prior to testing. Two knees from a whole lower extremity cadaver (age 50 years) were stored at -20°C and thawed at room temperature for 48 hours before testing. The ACL was transected and a medial menisectomy was performed on one knee while the other knee was left intact. Electromagnetic (EM) sensors were fixed to the injured knee to record kinematics during pivot shift testing. Gold standard knee kinematics and translation of the lateral knee compartment was recorded from an experienced surgeon prior to testing. After watching a two-minute instructional video on the standardized pivot shift test, sixteen subjects (n = 16; 3 orthopaedic surgeons, 2 sports medicine fellows, 4 residents, 3 athletic trainers and 4 medical students) performed ten trials of the standardized pivot shift test on both injured and control knees. Knee kinematics was captured using the sensors of an electromagnetic tracking system (Nest of Birds, Ascension Technology) fixed to the femur and tibia as previously reported [5]. Knee flexion angle, internal/external rotation, and varus/valgus values were determined during the applied pivot shift test. The 2D simple image analysis method was used to quantify anterior translation of the lateral knee compartment using a tablet computer and custom software as previously reported [2] These measurements were made for all sixteen subjects, ten trials each, while knee kinematics was collected for seven of the subjects. One-sample t-tests were used to compare recorded motions. Significance was set at $p<0.05$.

RESULTS: Overall, the anterior translation of the lateral knee compartment was significantly smaller than the gold standard values for both trials 1-5 and 6-10 in the injured knee ($p<0.05$, Table 1). The anterior translation of the lateral knee compartment for trials 1-5 and 6-10 decreased, diverging farther from gold standard values. No statistically significant difference in anterior translation of the lateral knee compartment was observed in the control knee for trials 1-5 nor 6-10 when compared to gold standard values, with improvement in difference from gold standard values noted. A statistically significant differences in the total range of flexion during the pivot shift test and almost double the total range of internal rotation were observed when compared to gold standard ($p <0.05$, Table 2). No significant difference was observed in applied range of varus/valgus rotation ($p = 0.65$).

DISCUSSION: This study examined the ability of participants to learn the standardized pivot shift test, via analysis of knee kinematics and anterior translation of the lateral knee compartment compared to a gold standard. While similar to the gold standard in the intact knee, subjects

demonstrated difficulty replicating the knee motion values representative of a standardized pivot shift test, and an inability to produce anterior translation of the lateral knee compartment comparable to gold standard values on an injured knee even after an instructional video. Ten trials were insufficient in allowing the subjects to learn and document performance improvement on the injured knee disproving the hypothesis under study. Future studies will assess passive and active instructional tools, a knee simulator as well as individualized feedback and critique of technique to develop the hand-eye skill to perform this clinical exam.

SIGNIFICANCE: This study provides useful information to surgeons and other clinicians regarding the ability to learn the standardized pivot shift test, using instructional video and paper instructions without receiving individual feedback or critique of technique.

REFERENCES: [1] Ayeni et al. KSSTA 2012 [2] Hoshino et al. KSSTA 2013 [3] Hoshino et al. KSSTA 2012 [4] Musahl et al. KSSTA 2012 [5] Grood et al. J Biomech Eng 1983

TABLES:

TABLES:

Table 1: Anterior translation of lateral knee compartment (mean)					
Knee	Trials	Subjects (mm)	Gold Standard (mm)	Absolute Difference (mm)	P-value (p <0.05)
Injured	1-5	3.0	8.4	5.4	p < 0.001
Injured	6-10	2.8		5.6	p <0.001
Control	1-5	1.5	1.7	0.3	p = 0.092
Control	6-10	1.6		0.2	p = 0.227

Table 2: Knee kinematics during standardized pivot shift test (mean (SD))				
Range of Motion	Gold Standard (SD)	Subjects (SD)	Difference (deg.)	P-value (p <0.05)
A) Flexion (deg.)	64.6 (2.6)	55.8 (5.6)	8.8	p = 0.016
B) Internal rotation (deg.)	44.1 (2.0)	23.0 (7.7)	21.1	p = 0.001
C) Valgus (deg.)	15.1 (0.3)	12.4 (11.2)	2.7	p = 0.650

Surface Strain in the Anterolateral Capsule of the Knee

Stephanie L. Sexton[1], Daniel Guenther[1,2], Kevin M. Bell[1], Sebastian Irarrazaval[1], Ata A. Rahnemai-Azar[1], Freddie H. Fu[1], Volker Musahl[1], Richard E. Debski[1]

[1]Orthopedic Robotics Laboratory, Departments of Orthopedic Surgery and Bioengineering, University of Pittsburgh, Pittsburgh, Pennsylvania, USA
[2]Trauma Department, Hannover Medical School (MHH), Hannover, Germany

Introduction: Knee injuries are one of the most common reasons for physician appointments. The most commonly injured ligament in the knee requiring surgery is the anterior cruciate ligament (ACL) [1]. ACL reconstruction is the sixth most common orthopedic surgical procedure in the US, with an estimated 150,000 ACL reconstructions performed annually [2]. However, injuries of the anterolateral capsule are often under diagnosed in conjunction to more common ACL procedures. Under diagnosis of anterolateral capsule injuries can lead to decreased rotational stability of the knee and early arthritis. Normal structure and function of the knee was restored in only 37% of the patients undergoing ACL reconstruction [3].

Significant clinical interest exists in anterolateral capsule-injuries with anterior cruciate ligament (ACL)-deficient knees and potential surgical treatment of the capsule at the time of ACL surgery [4]. Knowledge of the function of the anterolateral capsule can lead to development of an injury model and more informed choices of repair. Repair of the anterolateral capsule could increase ACL surgery success. The purpose of this study was to determine the surface strain of the anterolateral capsule in response to multiple loading conditions in the ACL intact and deficient knee during 30°, 60° and 90° of flexion. It was hypothesized that the greatest surface strain in the anterolateral capsule will be found at a 90-degree flexion angle with a combined internal rotation torque and anterior tibial load.

Methods: Six fresh frozen cadaveric knees (mean age 53.7 years, range 46-59 years) were dissected until the anterolateral capsule was clearly visible. Forty black markers were placed on the anterolateral capsule in a 5 x 8 grid beginning from Gerdy's tubercle posteriorly to the LCL insertion and from the LCL insertion superiorly to the LCL origin. The specimens were then loaded using a robotic testing system (MJT Model FRS2010, Chino, Japan). The femur was rigidly fixed relative to the lower plate of the robotic testing system and the tibia was attached to the upper end plate of the robotic manipulator through a 6-degree-of-freedom universal force/moment sensor (UFS, ATI Delta IP60 (SI-660-60), Apex, NC). The robot was used to apply loads to the knee at 3 flexion angles and a DMAS 7 Motion Capture System (Spica Technology Corporation, Haiku, HI) was utilized to track motion of the markers attached to the surface of the capsule. The loads were: Anterior Tibial Load, Combined Anterior Tibial Load and Internal Rotation Torque, External Rotation Torque, Combined External Rotation Torque with Varus Torque, Internal Rotation Torque, Combined Internal Rotation torque with Valgus Torque, Posterior Tibial Load, Combined Posterior Tibial Load with External Rotation Torque, Valgus Torque, and Varus Torque. The ten loading conditions were applied at 30°, 60°, and 90° of knee flexion for the intact and ACL deficient knee.

Peak maximum principal strain was computed by comparing the 3D marker positions in a non strained reference configuration to the loaded configurations using ABAQUS modeling software (Dassault Systems, Velizy-Villacoublay, France). The peak maximum principal strains computed by ABAQUS were averaged over the 6 specimens and compared with Students t-Tests. Two 2 tailed t-Tests with Bonferroni corrections were utilized to determine significance between flexion angles at each loading condition in both the ACL deficient and ACL Intact states. A one tailed t-Test compared the significance

16

of ACL deficient versus ACL Intact state for each loading condition at each flexion angle.

Results: Each specimen was found to have a different loading condition that produced the highest peak maximum principal strain. For all specimens the highest peak maximum principal strain of the anterolateral capsule was found between four loading conditions: Anterior Tibial Load, Combined Anterior Tibial Load with Internal Rotation Torque, Internal Rotation Torque, and Combined Internal Rotation Torque and Valgus Torque (Figure 1). The highest peak maximum principal strains were found in both ACL Intact and ACL deficient states. The ACL deficient state was generally found to have higher maximum principal strain than the ACL Intact state. Finally, higher flexion angles correlated with higher strains in the majority of loading conditions (Figure 2). For example, one maximum was found to be at 60° flexion with Internal Rotation Torque in the ACL deficient state.
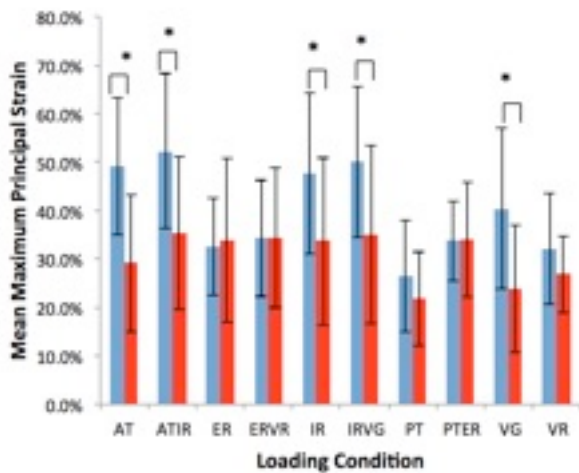

Figure 1. Mean Maximum Principal Strain at flexion angle of 30 degrees. AT = Anterior translation. ATIR = Anterior Translation + Internal rotation. ER = External rotation. ERVR = External rotation + Varus torque. IR = Internal rotation. IRVG = Internal rotation + Valgus torque. PT = Posterior translation. PTER = Posterior translation + External rotation. VG = Valgus torque. VR = Varus torque. Graph is representative of difference between loading conditions and ACL state at the same flexion angle. Blue = ACL deficient Red = ACL Intact. Statistically significant difference (*p<0.05)
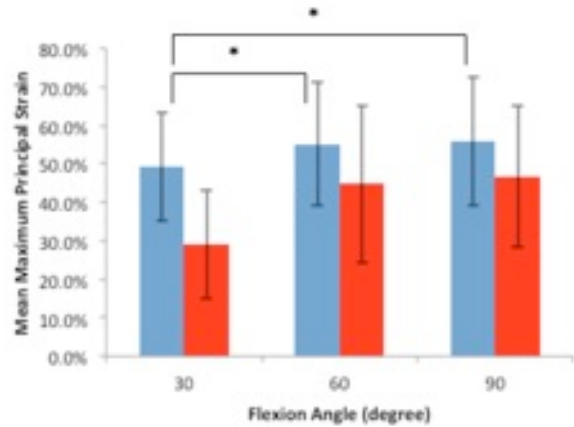

Figure 2. Mean Maximum Principal Strain during Anterior Tibial Load. Graph is representative of difference between flexion angle and ACL state during same loading condition with statistical difference between 30 and 60 degrees and 30 and 90 degrees. Blue=ACL deficient and Red = ACL Intact

Discussion: When comparing the ACL deficient and intact states there was a significant difference ($p < 0.05$) between 14 of the 30 compared states. In the ACL deficient state comparing the flexion angles 30 v 60 and 30 v 90 displayed statistical significance after application of a Bonferroni correction ($p < 0.0167$). The ACL intact knee flexion angles displayed minor statistically significant differences, only 4 of 30 compared states. When the ACL is deficient the strains on the anterolateral capsule are greater compared to when the ACL is intact because the capsule is acting as a primary restraint. Also, as the flexion angle of the knee increases from 30 to 60 and 30 to 90 the strains also increase as more load is accepted by the capsule when the ACL is deficient. Overall, when the ACL is intact less strain is placed on the anterolateral capsule. Finally, the values of the peak maximum principal strain were found to be much greater than the ultimate strains that can be held by tendons and ligaments. In conclusion, the anterolateral capsule in the ACL deficient state with higher flexion angles and four of the ten tested loading conditions results in the highest surface strain.

Significance: Understanding the loading conditions that most greatly strain the anterolateral capsule in knees with and without ACL damage will improve injury models. Knowledge of maximum principal strain patterns will also help surgeons to more accurately repair damage when both the ACL and the anterolateral capsule are damaged [4,5].

References:
1. Miyasaka et al. *Am J Knee Surg.,* **4**, 43–48, 1991

2. Spindler KP, Wright RW. *N Engl J Med.,* **359**(20):2135-2142, 2008
3. Biau et al. *Clin Orthop Relat Res.,* **458**:180-187, 2007
4. Guenther et al. Anterolateral rotatory instability of the knee. *Knee Surg Sports Traumatol Arthrosc.* 2015.
5. Moore et al. *Ann Biomed Eng* **38**(1):66-76, 2010

QUANTIFYING TIBIOFIBULAR KINEMATICS USING DMAS7 MOTION TRACKING SYSTEM TO INVESTIGAE SYNDESMOTIC INJURIES

Joseph M Takahashi[1], Kevin M Bell[1], MaCalus V Hogan[1,2] and Richard E Debski[1]

1. Department of Bioengineering, University of Pittsburgh, Pittsburgh, PA, United States.
2. Department of Orthopaedic Surgery, University of Pittsburgh, Pittsburgh, PA, United States.

INTRODUCTION

Injuries to the ankle syndesmosis, commonly referred to as high ankle sprains, typically occur as a result of external rotation or hyper dorsiflexion of the foot, which may disrupt the syndesmotic ligaments and compromise the integrity of the distal tibia, fibula, and talus [1]. Surgical treatment seeks to stabilize the distal tibiofibular structure to allow the syndesmosis to heal. Because an increase in fibula displacement relative to the tibia provides an effective method of determining a syndesmotic injury, quantifying such displacements are of immense interest clinically [2]. To quantify the rigid body motion between the tibia and fibula, a robotic testing system was used manipulate the foot relative to the tibia. However, an external system was necessary to track fibular motion. The objective of this study was to develop a protocol to develop a protocol to measure fibula motion using a motion capture system (DMAS7, Spicatek, HI) and assess the accuracy and repeatability of the methodology.

METHODS

In order to assess the DMAS7's ability to track kinematics,

- A mechanical digitizer was designed to register points in the DMAS7 system in order to create an anatomical coordinate system for the tibia and fibula
- Marker triads were designed to track kinematics.
- After validating the system, a practice test on a specimen was performed to determine a baseline for physiologic kinematics of the fibula.

Develop Mechanical Digitizer
The mechanical digitizer was validated based on its accuracy and repeatability. To evaluate repeatability, a bolt was digitized ten times and the difference of the x,y,z location of each point digitized and the average location of the ten points was determined.

Accuracy was determined by digitizing a bolt and then translating the bolt 2 mm. (Distance determined using a linear translator accurate to 10 μm).

Develop Marker Triads
A marker triad consisting of four contrast based markers (fourth marker for redundancy), was fixed to the robotic testing system, which displaced the triad three trials of 50 mm (large displacement) and rotated the triad three trials of 15° (large rotation). The camera system was validated based on its ability to accurately record these known displacements.

Track Physiological Motion
A cadaveric specimen with syndesmosis intact was mounted on the robotic testing system, preserving the syndesmosis. Marker triads were rigidly attached to the bone (Figure 1).
The medial and lateral malleoli, and two points located inferiorly and superiorly along the tibial crest were digitized to define the tibia anatomical
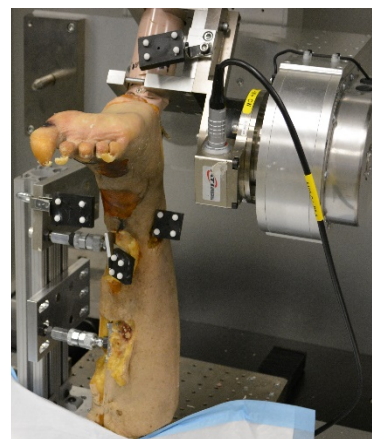

Figure 1: Set up to validate marker triads. Triads attached to tibia and fibula

coordinate system. Four loading conditions were simulated, each repeated three times to determine repeatability. Four testing conditions were applied: 10 Nm external rotation (ER) torque was applied at 0° of flexion, 10 Nm torque was applied to the ankle, 10 Nm ER torque was applied at 30° of plantarflexion as well as at 10° of dorsiflexion. The DMAS7 system was used to record the position of the marker triads at the endpoints of each testing condition.

Data Analysis

All video data was processed in the DMAS7 software to extract x,y,z coordinates of the tracked markers. All marker data was analyzed in Matlab (MathWorks Inc., MA). For both the mechanical digitizer and the marker triads, error associated with displacement and rotation was calculated as the absolute difference of the observed motion and the known motion.

VALIDATION CRITERIA

Average reported literature values for measured fibular displacement was found to be 2.35 mm [3]. Therefore, the validation criteria for accuracy and repeatability was set at ≤0.20 mm, an order of magnitude better. This validation criteria was applied to both the mechanical digitizer and tracking kinematics of the marker triads.

RESULTS

Mechanical Digitizer

The accuracy of the digitizer was determined to be 0.15 mm and repeatable to 0.11 mm.

Marker Triads

The error of the camera system for quantifying kinematics was found to be ≤ 0.66 mm for large displacements and ≤ 0.24 degrees for rotations (Figure 2**).**

Physiological Motion

For each physiological testing condition, variation in translation ranged from 0.04 mm to 0.69 mm (Table 1). In all testing conditions, medial lateral (ML) translation was observed, ranging from 0.66 – 1.51 mm (Table 1). Additionally, at least a 0.5 mm posterior displacement was observed during all testing conditions, which was especially prevalent during external rotation at 0° of flexion.
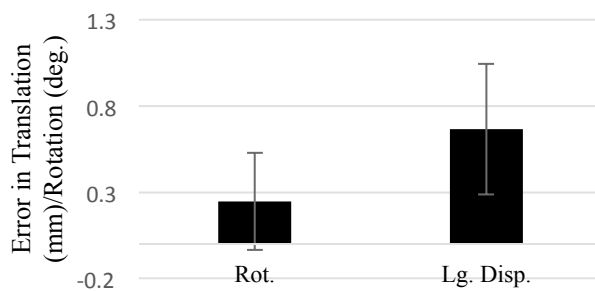

Figure 2: Error associated with large displacements and large rotations.

DISCUSSION

The design criteria established for accuracy and repeatability of the mechanical digitizer was 0.20 mm. The mechanical digitizer met the established design criteria for both accuracy and repeatability. Accuracy of tracking marker triads for large displacements and large rotations was greater than the established design criteria. However, 0.66 mm error for a large translations and rotation results in 1.32% and 1.86% error respectively, which was deemed to be acceptable at this time. Because expected fibular motion is small, further analysis will investigate the system accuracy for small translations and rotations.

Physiological Motion

Throughout all testing conditions, the variation between trials was on average 0.21 mm indicating the ability to perform physiological testing conditions to a high degree of repeatability. In all testing conditions performed, medial-lateral displacement (mortise widening) was observed. This is concurrent with some literature findings that report lateral displacement of the fibula [2] during syndesmotic injuries. While all testing conditions resulted in larger posterior displacements than reported in literature, a limitation of this study is that only one specimen was tested.

Future Directions

Upon completion of additional validation of the DMAS7 system, this methodology can be used in the analysis of additional ankle specimens to investigate syndesmotic injuries and repair procedures.

REFERENCES

1. Van Heest, T., Injuries to the Ankle Syndesmosis, JBJS, 2014:96 603-13.
2. Porter D., OAJSM, 2014:5 173-182.
3. Markolf, K., Syndesmotic Injuries, FAI, 2012:33 779 - 86.

ACKNOWLEDGEMENTS

Table 1: Fibular translations due to external rotation and maximum dorsiflexion

	Testing Condition			
Translation Direction	30° Plantarflex.+10 Nm ER	0° Flex.+10 Nm ER	10° Dorsiflex.+10 Nm ER	10 Nm Dorsiflex.
ML (mm) (+ = lateral)	1.36±0.06	1.51±0.06	1.60± 0.08	0.66±0.04
AP (mm) (+ = anterior)	-4.45±0.36	-6.02±0.38	-4.91±0.69	-0.55±0.30
SI (mm) (+ = superior)	-0.22±0.28	-0.39±0.08	-0.19±0.07	0.34±0.17